Springer

Journal of Mechanical Science and Technology 22 (2008) 2436~2444

Journal of Mechanical Science and Technology

www.springerlink.com/content/1738-494x
DOI 10.1007/s12206-008-0803-0

# Dynamics modeling and simulation of a new nine-bar press with hybrid-driven mechanism †

Hui Li[1,*], Yuping Zhang[1] and Haiqi Zheng[2]

[1]*Shijiazhuang Institute of Railway Technology, Dept. of Electromechanical Engineering, P. R. China*
[2] *Shijiazhuang Mechanical Engineering College, First Department, P. R. China*

(Manuscript Received March 11, 2008; Revised July 20, 2008; Accepted August 1, 2008)

**Abstract**

A novel hybrid-driven mechanical press for precision drawing is presented. This new press is composed of a nine-bar linkage which has two degrees of freedom determined by inputs from a dc constant speed motor and a dc servomotor. Therefore, the generalized coordinates are the angular displacement of two cranks. The kinetic energy, potential energy and generalized torques are analyzed. According to the equivalent circuit of the dc motor and the brushless servomotor, their dynamical model and position negative feedback model are developed separately. Then, a dynamical model for the hybrid-driven press is developed by using Lagrange's formulation. The dynamical equation is then transformed into a system of first order equations. Six first order differential equations are obtained in the state variables. In the end, the fourth fourth order Runge-Kutta method, an explicit method, is chosen as the integration technique of computer simulation. Two motors' current, two cranks' position and two cranks' angular velocity are treated as unknowns and the time response of the hybrid-driven press is obtained by integrating the system of first order equations through time.

*Keywords*: Hybrid-driven mechanism; Press; Dynamic formulation; Computer simulation; Servomotor; Mechatronics

## 1. Introduction

Mechanical presses are widely used in the metal industry. A crank press consisting of a slider-crank linkage is unsuitable for precision drawing because it lacks a constant working velocity [1]. Therefore, in order to obtain a constant working velocity, mechanical press manufacturers have developed multi-links presses. These attempts have focused on increasing the approach and return velocity. To slow down the slider velocity in the working stroke, it is important to obtain constant working speeds or make the load-stroke characteristics suitable for a special application. The multi-links presses, however, do not have flexibility for different drawing technology [2]. In order to provide for the more suitable load-stroke characteristics, many researchers have developed a flexible press which uses a servomotor as the prime mover [3-6]. However, the force capabilities of servomotors are usually limited. Recently, many researchers have paid more attention to a hybrid-driven mechanism. The main idea of hybrid-driven linkage is to combine the motion of a large constant velocity motor with a small servomotor via a two degree of freedom mechanism. The constant velocity motor provides the main power and motion requirement, while the servomotor acts as a low power motion modulation device. Therefore, the hybrid-driven linkage can provide for programmable motion output. The idea of hybrid-driven linkage was initially presented by Tokuz and Jones [7-10]. They used a differential gearbox as the hybrid mechanism to drive a slider-crank linkage. Greenough and Brashaw [11] took a seven bar mechanism as the hybrid linkage to generate a dwell

† This paper was recommended for publication in revised form by Associate Editor Hong Hee Yoo
*Corresponding author. Tel.: +86 311 8862 1089, Fax.: +86 311 8862 1073
E-mail address: Huili68@163.com

motion. Conner [12] synthesized a hybrid mechanism using a genetic algorithm. Kirecci and Dulger [13, 14] proposed a hybrid actuator. In the study, an arrangement consisting of a planar two degree of freedom, seven-link mechanism is driven by a constant speed motor and a servomotor. The dynamic behavior of hybrid actuator was studied by applying numerical simulation to the whole system. Lagrangian mechanics was applied to derive equations of motion. Simulation results were presented to demonstrate the ability of model developed with PID controller action. Herman [15] presented a hybrid cam mechanism. The hybrid cam mechanism adds much flexibility to the system requiring only small peak power and peak torque from the servomotor. Seth and Vaddi [16, 17] introduced the concept of programmable function generator mechanism. Li and Zhang [18, 19] investigated the feasibility of hybrid-driven mechanical presses. The scheme of a hybrid-driven mechanical press is put forward. A hybrid-driven nine-bar mechanical press for precision drawing is presented. The hybrid-driven mechanical press for precision drawing is optimized by a two step optimization. The dimension of the linkage and the motion rules of servomotor are obtained. By properly optimizing the displacement trajectory of the servomotor, the output motion of the slider can pass through the desired trajectories. Therefore, hybrid-driven mechanical presses have flexible output motion characteristics suitable for precision drawing. The advantages of a hybrid-driven mechanical press are analyzed.

In this study, the dynamics of a hybrid-driven nine-bar press, which is driven by a DC motor and a brushless servomotor, is studied by mathematical modeling and simulation. Then, the dynamic equations of this system are derived and solved numerically. The fourth fourth order Runge-Kutta method, an explicit method, is chosen as the integration technique of computer simulation. Simulation results are obtained for a motion profiles. In the end, the simulation results are presented and discussed.

## 2. Mathematical model for a hybrid-driven mechanical press

### *2.1 Forward kinematics analysis of hybrid-driven nine-bar press*

A hybrid-driven nine-bar press, shown in Fig. 1, is composed of a planar five-bar mechanism, a slider-crank linkage and a connection link. The crank $L_1$ is driven by a constant velocity motor. The crank $L_4$ is driven by a servomotor. Link $L_5$ is the fixed link. The $x$ -axis of the coordinate system in Fig. 1 is set along the vertical direction. The coordinate axes are fixed at point $A$. In order to improve the load characteristics of the slider, we take the point at which $L_{72}$ and $L_8$ are lined up in a straight line, at the BDC (Bottom Dead Center) of the slider and take BDC as the beginning point of the displacement.

According to Fig. 1, loop vector equations are given as follows:

$$\vec{L_1}+\vec{L_2}=\vec{L_5}+\vec{L_4}+\vec{L_3} \tag{1}$$

$$\vec{L_1}+\vec{L_2}=\vec{AG}+\vec{L_{71}}+\vec{L_6} \tag{2}$$

$$\vec{L_{72}}+\vec{L_8}=\vec{GF} \tag{3}$$

From Eq. (1)-(3), the following equations are obtained:

$$\begin{cases} L_1\cos\phi_1+L_2\cos\phi_2=L_5+L_4\cos\phi_4+L_3\cos\phi_3 \\ L_1\sin\phi_1+L_2\sin\phi_2=L_4\sin\phi_4+L_3\sin\phi_3 \\ L_1\cos\phi_1+L_2\cos\phi_2=x_G+L_{71}\cos\phi_{71}+L_6\cos\phi_6 \\ L_1\sin\phi_1+L_2\sin\phi_2=y_G+L_{71}\sin\phi_{71}+L_6\sin\phi_6 \\ L_{72}\cos(\phi_{71}+\delta)+L_8\cos\phi_8=S_0-S \\ L_{72}\sin(\phi_{71}+\delta)+L_8\sin\phi_8=0 \end{cases} \tag{4}$$

where $L_1$, $L_2$, $L_3$, $L_4$, $L_5$, $L_6$, $L_{71}$, $L_{72}$, $L_8$, $\delta$ are the dimension parameters of the mechanism as shown in Fig. 1. $S$ stands for the displacement function of the slide required by deep drawing process, $S=S(t)$; $S_0$ is given as follows:

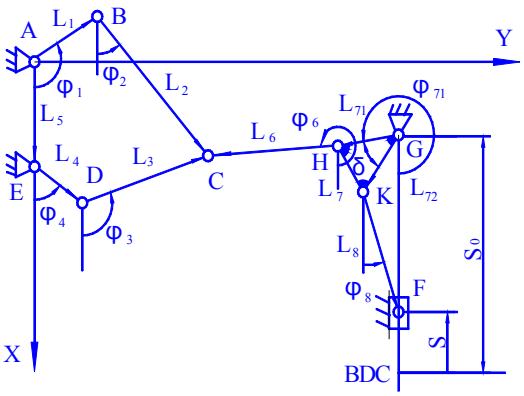


Fig. 1. Schematic drawing of the sample heat exchanger.

$$S_0 = L_{72} + L_8 \tag{5}$$

By solving Eq. (4), angular positions $\phi_2$, $\phi_3$, $\phi_4$, $\phi_6$, $\phi_{71}$, $\phi_8$ and slider displacement $S$ are obtained. Intermediate steps for the kinematics analysis can be seen in [20]. Having found the angular displacements of each link in the nine-bar linkage, time derivatives can be taken to find angular velocity and accelerations. They are definitely needed during the analysis of the dynamic model. They are given as follows:

$$\begin{cases} \omega_2 = \dfrac{L_4 \sin(\phi_3 - \phi_4)\omega_4 + L_1 \sin(\phi_1 - \phi_3)\omega_1}{L_2 \sin(\phi_3 - \phi_2)} \\ \omega_3 = \dfrac{L_4 \sin(\phi_2 - \phi_4)\omega_2 + L_1 \sin(\phi_1 - \phi_2)\omega_1}{L_3 \sin(\phi_3 - \phi_2)} \\ \omega_6 = \dfrac{L_1 \sin(\phi_1 - \phi_{71})\omega_1 + L_2 \sin(\phi_2 - \phi_{71})\omega_2}{L_6 \sin(\phi_6 - \phi_{71})} \\ \omega_7 = \dfrac{L_1 \sin(\phi_1 - \phi_6)\omega_1 + L_2 \sin(\phi_2 - \phi_6)\omega_2}{L_{71} \sin(\phi_{71} - \phi_6)} \\ \omega_8 = \dfrac{-L_{72}\omega_7 \cos(\phi_{71} + \delta)}{L_8 \cos\phi_8} \\ \dot{S} = L_{72} \sin(\phi_{71} + \delta)\omega_7 + L_8 \sin\phi_8 \omega_8 \end{cases} \tag{6}$$

$$\begin{cases} \varepsilon_2 = \dfrac{L_1\cos(\phi_1-\phi_3)\omega_1^2 + L_2\cos(\phi_2-\phi_3)\omega_2^2 - L_4\cos(\phi_4-\phi_3)\omega_4^2 - L_4\alpha_4^2 + L_4\sin(\phi_4-\phi_3)\varepsilon_4 - L_1\varepsilon_1\sin(\phi_3-\phi_1)}{L_2\sin(\phi_3-\phi_2)} \\ \varepsilon_3 = \dfrac{L_1\cos(\phi_1-\phi_2)\omega_1^2 - L_4\cos(\phi_4-\phi_2)\omega_4^2 - L_2\cos(\phi_4-\phi_2)\omega_2^2 + L_2\alpha_2^2 + L_4\sin(\phi_4-\phi_2)\varepsilon_4 - L_1\varepsilon_1\sin(\phi_2-\phi_1)}{L_3\sin(\phi_3-\phi_2)} \\ \varepsilon_6 = \dfrac{L_1\cos(\phi_1-\phi_{71})\omega_1^2 + L_2\cos(\phi_2-\phi_{71})\omega_2^2 - L_6\cos(\phi_6-\phi_{71})\omega_6^2 - L_{71}\omega_7^2 - L_2\sin(\phi_{71}-\phi_2)\varepsilon_2 - L_1\varepsilon_1\sin(\phi_{71}-\phi_1)}{L_6\sin(\phi_6-\phi_{71})} \\ \varepsilon_7 = \dfrac{L_1\cos(\phi_1-\phi_6)\omega_1^2 + L_2\cos(\phi_2-\phi_6)\omega_2^2 - L_{71}\cos(\phi_{71}-\phi_6)\omega_7^2 - L_6\alpha_6^2 - L_2\sin(\phi_6-\phi_2)\varepsilon_2 - L_1\varepsilon_1\sin(\phi_6-\phi_1)}{L_{71}\sin(\phi_{71}-\phi_6)} \\ \varepsilon_8 = \dfrac{-L_{72}\cos(\phi_{71}+\delta)\varepsilon_7 + L_{72}\sin(\phi_{71}+\delta)\omega_7^2 + L_8\sin\phi_8\omega_8^2}{L_8\cos\phi_8} \\ \ddot{S} = L_{72}\sin(\phi_{71}+\delta)\varepsilon_7 + L_{72}\cos(\phi_{71}+\delta)\omega_7^2 + L_8\sin\phi_8\varepsilon_8 + L_8\cos\phi_8\omega_8^2 \end{cases} \tag{7}$$

### *2.2 Coupled system equations for the nine-bar linkage*

A mathematical model for a nine-bar mechanism is developed by using Lagrange's formulation. The system's equation of motion is derived by using expressions for the system energy function, its partial and time derivatives with respect to the defined generalized coordinates. The mechanism operates in the vertical plane and gravity effects are included. Ideal operating conditions are assumed for modeling and computational ease, and motor loss effects are not included in the formulation.

In Fig. 1, $L_i$ denotes the length of the $i$th links. Using input angles $\phi_1$ and $\phi_4$ as the generalized coordinates describing the motion of the two DOF nine-bar mechanism ( $q_1 = \phi_1, q_2 = \phi_4$ ), Lagrange's equation can be given as

$$\frac{\mathrm{d}}{\mathrm{d}t}\left(\frac{\partial E}{\partial \dot{q}_k}\right) - \frac{\partial E}{\partial q_k} + \frac{\partial V}{\partial q_k} = Q_k \qquad (k = 1,2) \tag{8}$$

where $E$ is the kinetic energy, $V$ is the potential energy, $Q_k$ is the generalized torque on link 1 and link 4, and $q_k$ is the generalized coordinate.

The kinetic energy can be expressed as

$$E = \sum_{\substack{i=1 \\ i\neq 5}}^{9} \left[ \frac{1}{2} m_i \left( \dot{x}_{Si}^2 + \dot{y}_{Si}^2 \right) + \frac{1}{2} J_i \dot{\phi}_i^2 \right] \tag{9}$$

where $\dot{\phi}_i$ is the angular velocity of link $i$, $\dot{x}_{Si}$ and $\dot{y}_{Si}$ are the $x$ and $y$ velocity components of its center of mass of link $i$. Then, $\dot{\phi}_i$, $\dot{x}_{Si}$ and $\dot{y}_{Si}$ can be written as

$$\dot{\phi}_i = \frac{\partial \phi_i}{\partial q_1}\dot{q}_1 + \frac{\partial \phi_i}{\partial q_2}\dot{q}_2 \tag{10}$$

$$\begin{cases} \dot{x}_{Si} = \dfrac{\partial x_{Si}}{\partial q_1}\dot{q}_1 + \dfrac{\partial x_{Si}}{\partial q_2}\dot{q}_2 \\ \dot{y}_{Si} = \dfrac{\partial y_{Si}}{\partial q_1}\dot{q}_1 + \dfrac{\partial y_{Si}}{\partial q_2}\dot{q}_2 \end{cases} \tag{11}$$

By substituting Eq. (3) and (4) into Eq. (1),

$$E = \frac{1}{2} J_{11} \dot{q}_1^{\,2} + J_{12}\dot{q}_1\dot{q}_2 + \frac{1}{2} J_{22}\dot{q}_2^2 \tag{12}$$

where $J_{11}$´ $J_{12}$´ $J_{22}$ are the equivalent moment of inertia of the two DOF nine-bar mechanism. These relationships are included in the Appendix.

The potential energy of the mechanism can be expressed as

$$\begin{aligned} V = &-m_1 g x_{S1} - m_2 g x_{S2} - m_3 g x_{S3} - m_4 g x_{S4} \\ &- m_6 g x_{S6} - m_7 g x_{S7} - m_8 g x_{S8} - m_9 g x_{S9} \end{aligned} \tag{13}$$

where $m_i$ represents the mass of the link $i$, $g$ represents the gravity constant, $x_{Si}$ represents the location of the centers of mass of the link $i$ in axis $x$, and $S$ represents the displacement of the slider.

According to the principle of virtual work, the generalized torque $Q_k$ can be given as

$$\begin{bmatrix} Q_1 \\ Q_2 \end{bmatrix} = \begin{bmatrix} M_{d1} + Q\dfrac{\partial S}{\partial q_1} \\ M_{d4} + Q\dfrac{\partial S}{\partial q_2} \end{bmatrix} \tag{14}$$

where $M_{d1}$ is the external input torque on the crank

$L_1$, $M_{d4}$ is the external input torque on the crank $L_4$, and $Q$ is the forming force of the slider.

Differentiating Eq. (12) and (13) and substituting them into Eq. (8), yields

$$\begin{bmatrix} Q_1 \\ Q_2 \end{bmatrix} = \begin{bmatrix} J_{11}\ddot{q}_1 + J_{12}\ddot{q}_2 + \frac{1}{2}\frac{\partial J_{11}}{\partial q_1}\dot{q}_1^2 + \frac{\partial J_{11}}{\partial q_2}\dot{q}_1\dot{q}_2 \\ \quad + \left(\frac{\partial J_{12}}{\partial q_2} - \frac{1}{2}\frac{\partial J_{22}}{\partial q_1}\right)\dot{q}_2^2 + \frac{\partial V}{\partial q_1} \\ J_{22}\ddot{q}_2 + J_{12}\ddot{q}_1 + \left(\frac{\partial J_{12}}{\partial q_1} - \frac{1}{2}\frac{\partial J_{11}}{\partial q_2}\right)\dot{q}_1^2 \\ \quad + \frac{\partial J_{12}}{\partial q_1}\dot{q}_1\dot{q}_2 + \frac{1}{2}\frac{\partial J_{22}}{\partial q_2}\dot{q}_2^2 + \frac{\partial V}{\partial q_2} \end{bmatrix} \quad (15)$$

This is a second order, nonlinear differential equations system describing the mechanism motion as represented by generalized coordinates $q_1$ and $q_2$. Eq. (15) is the coupled equations. Intermediate steps of derivation and the derivate terms can be found in [20].

Eq. (15) can be transformed into,

$$\begin{cases} \ddot{q}_1 = A_0 + A_{11}\dot{q}_1^2 + A_{12}\dot{q}_1\dot{q}_2 + A_{22}\dot{q}_2^2 \\ \ddot{q}_2 = B_0 + B_{11}\dot{q}_1^2 + B_{12}\dot{q}_1\dot{q}_2 + B_{22}\dot{q}_2^2 \end{cases} \quad (16)$$

where $A_0$, $B_0$, $A_{11}$, $B_{11}$, $A_{12}$, $B_{12}$, $A_{22}$, $B_{22}$ are the coefficients of the second order differential equation. These coefficients are given in the Appendix.

### *2.3 Mathematical model for the DC motors*

Fig. 2 shows a DC motor, including a geared speed-reducer having a gear ratio of

$$n_k = \frac{T_{bk}}{T_{ak}} = \frac{\omega_{ak}}{\omega_{bk}} \quad (k = 1, 2) \quad (17)$$

where $\omega_{ak}$ is the angular velocity of the input shaft

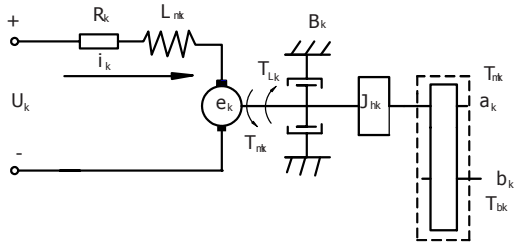


Fig. 2. Geometric details of the fin and tube.

$a_k$, $\omega_{bk}$ is the angular velocity of output shaft $b_k$. In Fig. 2, the input to the motor-gear system is voltage $U_k$, and the output of the system is the torque $T_{bk}$ which is equal to $M_{dk}$ as defined in Eq.(14). $R_k$, $L_k$, $i_k$ are the armature resistance, inductance and current, respectively. The shaft $b_k$ is connected to drive the crank $L_1$ and crank $L_4$ of the mechanism, respectively. $B_k$ is a damping coefficient due to a possible viscous bearing friction, $T_{Lk}$ is a constant mechanical load, due to brush friction, gear friction or dry bearing friction , for instance. $J_{hk}$ is the combined moment of inertia of the motor rotor , the speed reducer, and the flywheel. Since two different DC motor types are studied, the same motor equations are used and the different motor data are utilized. Here $k$ is equal to 1 for a DC motor and 2 for a brushless servomotor, respectively, throughout the work. $J_{hk}$ is given as follows:

$$J_{hk} = J_{mk} + J_{Rk} + J_{fk} \quad (18)$$

where $J_{mk}$ is the moment of inertia of the motor rotor, $J_{Rk}$ is the equivalent moment of inertia of the speed reducer, $J_{fk}$ is the moment of inertia of the flywheel.

From Kirchhoff's voltage law,

$$U_k = R_k i_k + L_{mk}\frac{\mathrm{d}i_i}{\mathrm{d}t} + e_k \quad (19)$$

where $e_k$ is the generated electromotive force of the motor.

Using a Newtonian equation for the mechanical load, we have

$$T_{bk} = n_k(T_{mk} - T_{Lk} - B_k\omega_{ak} - J_{hk}\frac{\mathrm{d}\omega_{ak}}{\mathrm{d}t}) \quad (20)$$

where $T_{mk}$ is the magnetic motor torque, $n_k$ is the gear ratio defined by Eq. (17). The magnetic torque and the generated electromotive force are given as,

$$T_{mk} = k_{tk} i_k \quad (21)$$

$$e_k = k_{ek}\omega_{ak} \quad (22)$$

where $k_{tk}$ is the motor torque constant, and $k_{ek}$ is the motor voltage constant. Observing that

$$\omega_{ak} = n_k\omega_{bk} = n_k\dot{q}_k \quad (23)$$

Substituting Eqs. (21)-(23) into Eqs. (19) and (20), we find

$$\frac{di_k}{dt} = \frac{U_k - R_k i_k - n_k k_{ek}\dot{q}_k}{L_{mk}} \tag{24}$$

$$T_{bk} = n_k k_{tk} i_k - n_k T_{Lk} - n_k^2 B_k \dot{q}_k - n_k^2 J_{hk}\ddot{q}_k \tag{25}$$

Eqs. (24) and (25) are the mathematical models of the motor dynamics.

When the motor is controlled by the PID position closed loop, the voltage $U_i$ can be given as

$$U_k = k_{pk}(q_{kic} - q_k) + k_{dk}(\dot{q}_{kic} - \dot{q}_k) + k_{Ik}\int_0^t (q_{Kc} - q_k)dt \tag{26}$$

where $k_{pk}$ is the proportional gain constant, $k_{dk}$ is the derivative gain constant, $k_{Ik}$ is the integral gain constant. $q_{kc}$ and $\dot{q}_{kc}$ are the ideal angular displacement and ideal angular velocity of the crank $L_k$ respectively, and $q_k$ and $\dot{q}_k$ are the actual angular displacement and actual angular velocity of the crank $L_k$, respectively.

Substituting Eq. (26) into Eq. (24),

$$\frac{\mathrm{d}i_k}{\mathrm{d}t} = \frac{\left(k_{pk}(q_{kc} - q_k) + k_{dk}(\dot{q}_{kc} - \dot{q}_k) + k_{Ik}\int_0^t (q_{kic} - q_k)dt\right) - R_k i_k - n_k k_{ek}\dot{q}_k}{L_{mk}} \quad (k=1,2) \tag{27}$$

Eq. (27) is the PID control model of the servomotor dynamics. The proportional gain constant $k_{pk}$, the derivative gain constant $k_{dk}$ and the integral gain constant $k_{Ik}$ are optimized by running the simulation software with real mechanism parameters and motor data [20].

### *2.4 Mathematical model for the electromechanical coupled system of the press*

Combining Eq. (16) and (27),

$$\begin{cases} \ddot{q}_1 = A_0 + A_{11}\dot{q}_1^2 + A_{12}\dot{q}_1\dot{q}_2 + A_{22}\dot{q}_2^2 \\ \ddot{q}_2 = B_0 + B_{11}\dot{q}_1^2 + B_{12}\dot{q}_1\dot{q}_2 + B_{22}\dot{q}_2^2 \\ \dfrac{\mathrm{d}i_1}{\mathrm{d}t} = \dfrac{\left(k_{p1}(q_{1c} - q_1) + k_{d1}(\dot{q}_{1c} - \dot{q}_1) + k_{I1}\int_0^t (q_{1c} - q_1)dt\right) - R_1 i_1 - n_1 k_{e1}\dot{q}_1}{L_{m1}} \\ \dfrac{\mathrm{d}i_2}{\mathrm{d}t} = \dfrac{\left(k_{p2}(q_{2c} - q_2) + k_{d2}(\dot{q}_{2c} - \dot{q}_2) + k_{I2}\int_0^t (q_{2c} - q_2)dt\right) - R_2 i_2 - n_2 k_{e2}\dot{q}_2}{L_{m2}} \end{cases} \tag{28}$$

Let,

$$x_1 = q_1, x_2 = q_2, x_3 = \dot{q}_1, x_4 = \dot{q}_2, x_5 = i_1, x_6 = i_2$$

Then, Eq. (28) can be transformed into a system of first order equations,

$$\begin{cases} \dot{x}_1 = x_3 \\ \dot{x}_2 = x_4 \\ \dot{x}_3 = A_0 + A_{11}x_3^2 + A_{12}x_3x_4 + A_{22}x_4^2 \\ \dot{x}_4 = B_0 + B_{11}x_3^2 + B_{12}x_3x_4 + B_{22}x_4^2 \\ \dot{x}_5 = \dfrac{\left(k_{p1}(\phi_{1c} - x_1) + k_{d1}(\dot{\phi}_{1c} - x_3) + k_{I1}\int_0^t (\phi_{1c} - x_1)dt\right) - R_1 x_5 - n_1 k_{e1} x_3}{L_{m1}} \\ \dot{x}_6 = \dfrac{\left(k_{p2}(\phi_{4c} - x_2) + k_{d2}(\dot{\phi}_{4c} - x_4) + k_{I1}\int_0^t (\phi_{4c} - x_2)dt\right) - R_2 x_6 - n_2 k_{e2} x_4}{L_{m2}} \end{cases} \tag{29}$$

## 3. Simulation results and discussion

The dynamic behavior of this system is studied by using numerical methods. The fourth order Runge-Kutta method is chosen as the integration technique. This is commonly employed method for integration of the a system of nonlinear equations. The motor current, the angular displacement, and the angular velocity of the crank are treated as unknowns, and the time response of the motor-mechanism system is obtained by integrating the system of first order equations through time.

The initial constant for the variables in Eq. (29) is zero. The motor and mechanism parameters of the hybrid driven press are given in Table 1, Table 2 [21] and Table 3. The gear ratios $n_1$ and $n_2$ defined in Eq. (17) are 10 and 20, respectively. The equivalent moment of inertia $J_{R1} + J_{f1}$ defined in Eq. (18) is equal to $32\ kgm^2$. The proportional gain constant and derivative gain constant are obtained by using optimization technique [20]. The optimum results are found to be $[k_{p1}, k_{d1}, k_{I1}]^T = [270.2, 3.4, 0]^T$ and $[k_{p2}, k_{d2}, k_{I2}]^T = [180.5, 2.67, 0]^T$, respectively. The motion cycle is 0.6 second and the simulation time is taken as two motion cycles. The simulation time step is 0.1667ms. The forming force of the press is given in Fig. 3. Since zero initial conditions are given for the motor current, the crank angle displacement and the crank angular velocity, transients are observed in the simulation results. The steady-state is then achieved in one motion cycle. Fig. 4(a), (b), (c) show the simulation results for the crank $L_1$ (angular displacement, velocity, acceleration). The constant speed motor rotates at 1000 rpm and crank

Table 1. DC motor parameters.

| | |
|---|---|
| DC motor model | $Z_4-132-2$ |
| Rated power $P_e$ | 11 KW |
| Rated voltage $U_e$ | 440 V |
| Rated current $I_e$ | 30.7 A |
| Rated speed/maximum speed $n_e / n_{\max}$ | 1000/2000 r/min |
| Moment of inertia $GD^2$ | 1.6 kg.m$^2$ |
| Winding resistance $R_1$ | 1.62 $\Omega$ |
| Winding inductance $L_{m1}$ | $7.8\times10^{-3}$ H |
| Motor voltage constant $k_{e1}$ | 5.7 V/rad/s |
| Motor torque constant $k_{t1}$ | 4.3572 Nm/A |
| Efficiency $\eta$ | 88.7% |

Table 2. DC servo motor parameters.

| | |
|---|---|
| Rated power $P_e$ | 3 KW |
| Maximum operating speed $n_{\max}$ | 3000 r/min |
| Rotor moment of inertia $J_{m2}$ | $6.8\times10^{-4}$ kg.m$^2$ |
| Winding resistance $R_2$ | 0.8$\Omega$ |
| Winding inductance $L_{m2}$ | $5.8\times10^{-3}$ H |
| Motor voltage constant $k_{e2}$ | 0.8598 V/rad/s |
| Motor torque constant $k_{t2}$ | 0.76 Nm/A |
| Continuous stall torque $T_e$ | 10.2 Nm |
| Peak torque $T_p$ | 19.7 Nm |

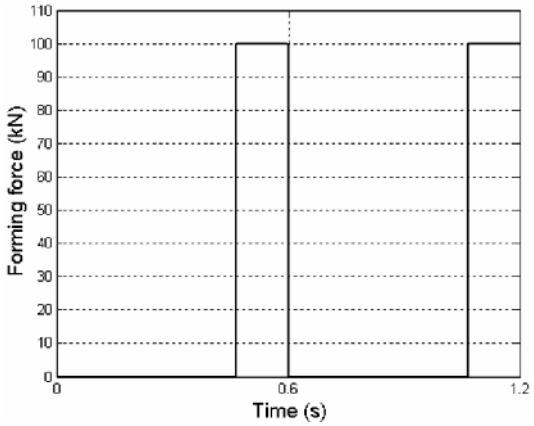


Fig. 3. Schematic drawing of the test facility.

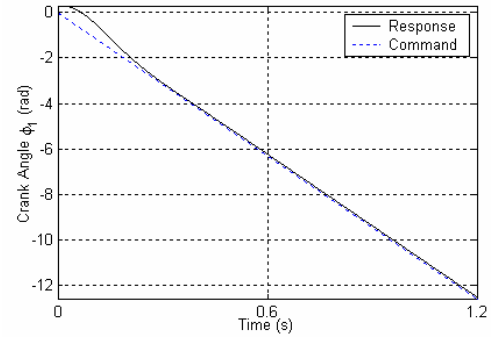


(a) Crank angle $\phi_1$

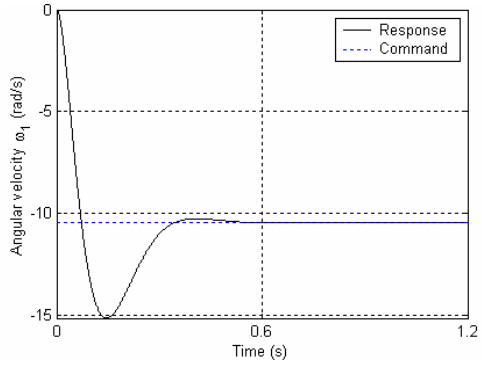


(b) Angular velocity $\omega_1$

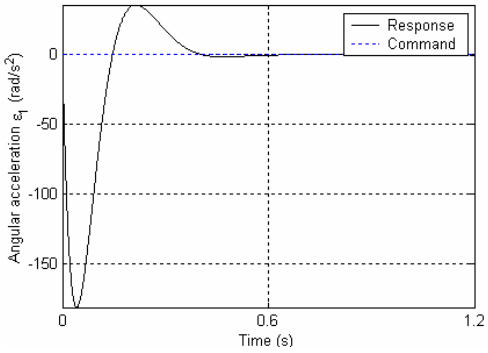


(c) Angular acceleration $\varepsilon_1$

Fig. 4. Sketch showing the installation of the sample.

Table 3. Nine-bar mechanism parameters.

| parameters | Link 1 | Link 2 | Link 3 | Link 4 | frame 5 | Link 6 | Link71 | Link72 | Link 8 | Slider7 | $\delta$ |
|---|---|---|---|---|---|---|---|---|---|---|---|
| Link length $L_i$ (mm) | 54.2 | 423.2 | 423.2 | 53.2 | 423.2 | 216.1 | 216.1 | 284.55 | 324.15 | | 28.3 |
| Radius $r_i$ (m) | 0.025 | 0.025 | 0.025 | 0.025 | | 0.025 | 0.025 | 0.025 | 0.025 | | |
| Mass $m_i$ (kg) | 0.1323 | 1.037 | 1.037 | 0.1323 | | 0.5295 | 0.5295 | 0.6973 | 0.7943 | 20 | |
| Moment of inertia $J_i$ (kg.m$^2$) | 0.3043 | 0.1548 | 0.1548 | 0.0076 | | 4.2721 | 0.0595 | | 0.0069 | | |

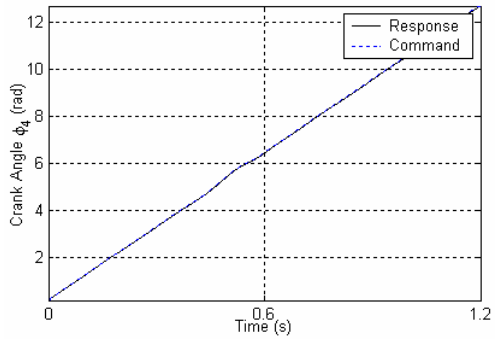


(a) Crank angle $\phi_4$

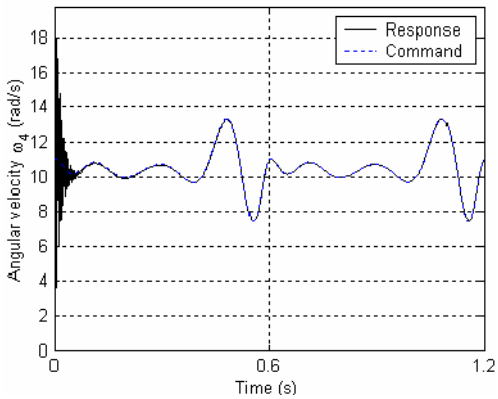


(b) Angular velocity $\omega_4$

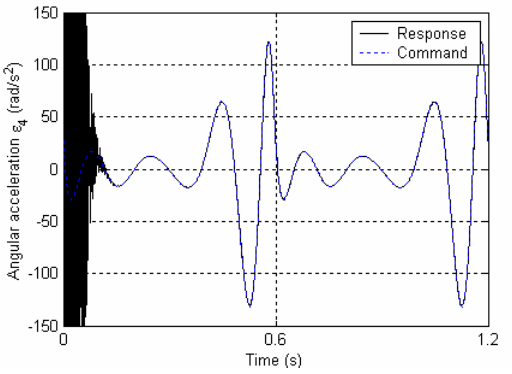


(c) Angular acceleration $\varepsilon_4$

Fig. 5. Sketch of typical condensate drainage patterns.

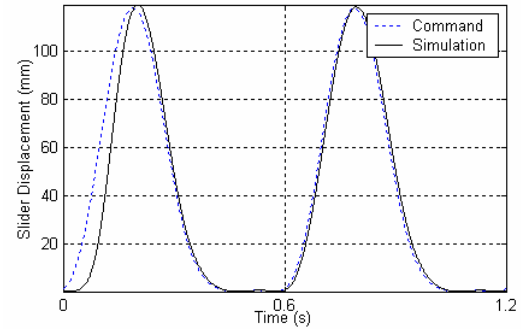


(a) Slider displacement

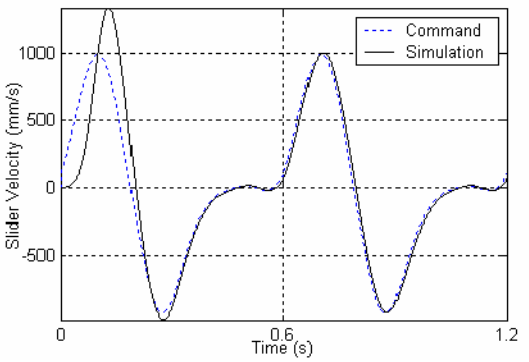


(b) Slider velocity

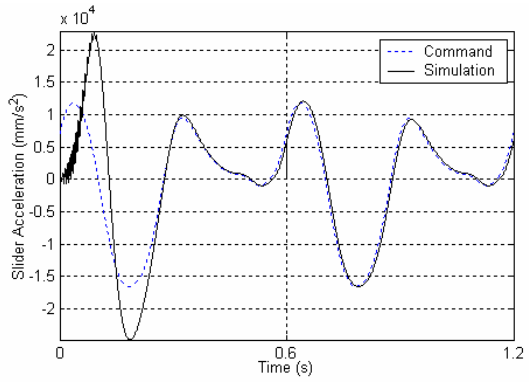


(c) Slider acceleration

Fig. 6. Effect of inclination angle on j and f factors.

$L_1$ has 100 rpm at the end. Fig. 5(a), (b), (c) show the simulation results for the crank $L_4$ (angular displacement, velocity, acceleration). Fig. 6(a), (b), (c) show the simulation results for the slider (slider displacement, velocity and acceleration). The observation is made from Fig. 4(a), (b), (c), that the output velocity, acceleration response curve of the constant speed motor is regarded as oscillatory. This behavior is simply caused by initial conditions given as zero and the effect of the forming force. The tracking performances for angular displacement, velocity of crank $L_4$ driven by the servomotor is very good in the second cycle. Simulation results of the slider are well correlated with the reference points.

## 4. Conclusion

In this work, the theoretical investigation of a hybrid-driven press with its dynamics has been described. A study was performed to model, simulate and control a hybrid-driven precision press driven by a dc motor and a brushless servomotor. According to the Lagrange equation, a mathematical model for the hybrid-driven press was developed. Then the mathematical model was solved and simulated by using numerical method. Better correlations between the simulated results and given command were obtained. Therefore, the feasibility of the hybrid-driven press for precision drawing is verified in theory and by computer simulation.

## Acknowledgments

The authors are grateful to the National Natural Science Foundation of China for supporting this research under grant No.50775219 and No. 50375157.

## References

[1] D. He, *Crank presses,* China Machine Press, Beijing, China (1987).

[2] D. He, *Special presses,* China Machine Press, Beijing, China (1989).

[3] Yan Hongsen and Chen Weiren, A variable input speed approach for improving the output motion characteristics of watt-type presses, *International Journal of Machine Tools & Manufacture*, 40 (5) (2000) 675-690.

[4] S. Yossifon and R. Shivpuri, Analysis and comparison of selected rotary linkage drives for mechanical presses, *International Journal of Machine Tools & Manufacture*, 33 (2) (1993) 175-192.

[5] S. Yossifon and R. Shivpuri, Design considerations for the electric servo motor driven 30 ton double knuckle press for precision forming, *International Journal of Machine Tools & Manufacture*, 33 (2) (1993) 193-208.

[6] S. Yossifon and R. Shivpuri, Optimization of a double knuckle linkage drive with constant mechanical advantage for mechanical presses, *International Journal of Machine Tools & Manufacture*, 33 (2) (1993) 209-222.

[7] L. C. Tokuz and J. R. Jones, Programmable modulation of motion using hybrid machine, *Proceeding of Im*eche, C414/071 (1991) 85-92.

[8] L. C. Tokuz, *Hybrid machine modeling and control,* Ph.D. Thesis, Department of Mech., Liverpool Polytechnic, UK, (1992).

[9] L. C. Tokuz and J. R. Jones, Power transmission and flow in the hybrid machines, *The 6th International Machine Design and Production Conference*, MENU, ANKARA, TURKEY, (1994) 209-218.

[10] L. C. Tokuz and J. R. Jones, A design guide for hybrid machine applications, *Transactions Journal of Engineering and Environment Sciences*, 21 (1997) 1-11.

[11] J. D.Greenough, et al, Design of hybrid machine, *Proceedings of the 9th IFToMM world Congress*, (1995) 2501-2505.

[12] A. M. Conner et al, The synthesis of hybrid five-bar path generating mechanisms using genetic algorithms, *Genetic Algorithms in Engineering System: Innovations and Application*, (1995) 313-318.

[13] Ali Kirecci and L. Canan Dulger, A study on a hybrid actuator, *Mechanism and Machine Theory*, 35 (8) (2000) 1141-1149.

[14] L. C. Dulger, Ali Kirecci and M. Topalbekiroglu, Modeling and simulation of a hybrid actuator, *Mechanism and Machine Theory*, 38 (5) (2003) 395-407.

[15] J. Herman, V. De Straete and J. De Schutter, Hybrid cam mechanism, *IEEE/ASME Transactions on Mechatronics*, 1 (4) (1996) 284-289.

[16] Bhartendu Seth and Sesha Sai Vaddi, Programmable function generators- Ⅰ: Base five-bar mechanism, *Mechanism and Machine Theory*, 38 (4) (2003) 321-330.

[17] Sesha Sai Vaddi and Bhartendu Seth, Programmable function generators- Ⅱ: seven-bar translatory-out mechanism, *Mechanism and Machine Theory*, 38 (4) (2003) 331-343.

[18] Hui Li and Ce Zhang, Reaearch on the feasibility of hybrid-driven mechanical press. *Mechanical Science and Technology*, 23 (10) (2004) 1253-1256.

[19] Hui Li, Ce Zhang and Caifang Meng, A hybrid-driven nine-bar press for precision drawing, *Proceedings of the 11th World Congress in Mechanism and Machine Science*, Tianjin, China, (2004) 1141-1145.

[20] Hui Li, *Fundamental study on the hybrid-driven programmable mechanical press*, Ph.D. Thesis, Tianjin University, Tianjin, China, (2003).

[21] W. M. Hwang, Y. C. Hwang and S. T. Chiou, A drag-link drive of mechanical presses for precision drawing, *International Journal of Machine Tools & Manufacture*, 35 (10) (1995) 1425-1433.

## Appendix

The kinetic energy $E$ can be expressed as,

$$E=\sum_{\substack{j=1\\ j\neq 5}}^{9}\frac{1}{2}\left\{m_j\left[\left(\frac{\partial x_{Sj}}{\partial q_1}\right)^2+\left(\frac{\partial y_{Sj}}{\partial q_1}\right)^2\right]+J_j\left(\frac{\partial \phi_j}{\partial q_1}\right)^2\right\}\dot{q}_1^2+\sum_{\substack{j=1\\ j\neq 5}}^{9}\frac{1}{2}\left\{m_j\left[\left(\frac{\partial x_{Sj}}{\partial q_2}\right)^2+\left(\frac{\partial y_{Sj}}{\partial q_2}\right)^2\right]+J_j\left(\frac{\partial \phi_i}{\partial q_2}\right)^2\right\}\dot{q}_2^2+\sum_{\substack{j=1\\ j\neq 5}}^{9}\frac{1}{2}\left\{m_j\left[\left(\frac{\partial x_{Sj}}{\partial q_1}\frac{\partial x_{Sj}}{\partial q_2}+\frac{\partial y_{Sj}}{\partial q_1}\frac{\partial y_{Sj}}{\partial q_2}\right)\right]+J_j\left(\frac{\partial \phi_j}{\partial q_1}\frac{\partial \phi_j}{\partial q_2}\right)\right\}\dot{q}_1\dot{q}_2$$

where

$$J_{11}=\sum_{\substack{j=1\\ j\neq 5}}^{9}\left\{m_j\left[\left(\frac{\partial x_{Sj}}{\partial q_1}\right)^2+\left(\frac{\partial y_{Sj}}{\partial q_1}\right)^2\right]+J_j\left(\frac{\partial \phi_j}{\partial q_1}\right)^2\right\}$$

$$J_{12}=\sum_{\substack{j=1\\ j\neq 5}}^{9}\left\{m_j\left[\left(\frac{\partial x_{Sj}}{\partial q_1}\frac{\partial x_{Sj}}{\partial q_2}+\frac{\partial y_{Sj}}{\partial q_1}\frac{\partial y_{Sj}}{\partial q_2}\right)\right]+J_j\left(\frac{\partial \phi_j}{\partial q_1}\frac{\partial \phi_j}{\partial q_2}\right)\right\}$$

$$J_{22}=\sum_{\substack{j=1\\ j\neq 5}}^{9}\left\{m_j\left[\left(\frac{\partial x_{Sj}}{\partial q_2}\right)^2+\left(\frac{\partial y_{Sj}}{\partial q_2}\right)^2\right]+J_j\left(\frac{\partial \phi_i}{\partial q_2}\right)^2\right\}$$

Explicit forms of $A_0$, $B_0$, $A_{11}$, $B_{11}$, $A_{12}$, $B_{12}$, $A_{22}$, $B_{22}$ are given as follows:

$$A_0=(Q_1J_{22}-Q_2J_{12})/C_1$$

$$B_0=(Q_2J_{11}-Q_1J_{12})/C_1$$

$$C_1=J_{11}J_{22}-J_{12}^2$$

$$A_{11}=\left[J_{12}\frac{\partial J_{12}}{\partial q_1}-\frac{1}{2}J_{12}\frac{\partial J_{11}}{\partial q_2}-\frac{1}{2}J_{22}\frac{\partial J_{11}}{\partial q_1}\right]\frac{1}{C_1}$$

$$B_{11}=\left[-J_{11}\frac{\partial J_{12}}{\partial q_1}+\frac{1}{2}J_{12}\frac{\partial J_{11}}{\partial q_1}+\frac{1}{2}J_{11}\frac{\partial J_{11}}{\partial q_2}\right]\frac{1}{C_1}$$

$$A_{12}=\left[J_{12}\frac{\partial J_{22}}{\partial q_1}-J_{22}\frac{\partial J_{11}}{\partial q_2}\right]\frac{1}{C_1}$$

$$B_{12}=\left[J_{12}\frac{\partial J_{11}}{\partial q_2}-J_{11}\frac{\partial J_{22}}{\partial q_1}\right]\frac{1}{C_1}$$

$$A_{22}=\left[\frac{1}{2}J_{12}\frac{\partial J_{22}}{\partial q_2}-J_{22}\frac{\partial J_{12}}{\partial q_2}+\frac{1}{2}J_{22}\frac{\partial J_{22}}{\partial q_1}\right]\frac{1}{C_1}$$

$$B_{22}=\left[-\frac{1}{2}J_{12}\frac{\partial J_{22}}{\partial q_1}+J_{12}\frac{\partial J_{12}}{\partial q_2}-\frac{1}{2}J_{11}\frac{\partial J_{22}}{\partial q_2}\right]\frac{1}{C_1}$$

**Hui Li** received the B.S. degree in mechanical engineering from the Hebei Polytechnic University, Hebei, China, in 1991. He received the M.S. degree in mechanical engineering from the Harbin University of Science and Technology, Heilongjiang, China, in 1994. He received the PhD degree from the School of Mechanical Engineering of Tianjin University, Tianjin, China, in 2003. He is currently a professor in mechanical engineering at Shijiazhuang Institute of Railway Technology, China. His research and teaching interests include hybrid driven mechanism, kinematics and dynamics of machinery, mechatronics, CAD/CAPP, signal processing for machine health monitoring, diagnosis and prognosis.